Extra-framework zirconium clusters in Metal Organic Framework DUT-67 controlled by the choice of the metal precursor

*Nicola Precisvalle[1,†], Phuoc Hoang Ho[2,†], Thomas Cacciaguerra[2], Stefano Deabate[3], Luc Girard[4], Guillaume Toquer[4], Khoa D. Nguyen[5,6], Ha Vu Le[5,6], Francesco Di Renzo[2], Annalisa Martucci[1] *, Philippe Trens[2] **

[1] Department of Physics and Earth Sciences, University of Ferrara, Ferrara, Italy

[2] ICGM, Univ Montpellier, CNRS, ENSCM, Montpellier, France.

[3] IEM, Univ Montpellier, CNRS, ENSCM, Montpellier, France.

[4] ICSM, Univ Montpellier, CEA, CNRS, ENSCM, Marcoule, France

[5] Department of Chemical Engineering, Ho Chi Minh University of Technology, 268 Ly Thuong Kiet street, District 10, Ho Chi Minh City, Vietnam.

[6] Vietnam National University Ho Chi Minh City, Linh Trung Ward, Thu Duc District, Ho Chi Minh City, Vietnam.

[†] Equal contribution

Keywords: DUT-67, Extra-framework clusters, Rietveld structure refinement, Zr-MOF, Zirconium precursors

Abstract

DUT-67 zirconium-thiophenedicarboxylate (TDC) MOFs have been synthesized in the presence of formic acid from different zirconium precursors. The materials formed have been

characterized by X-ray diffraction, nitrogen sorption, scanning electron microscopy, and thermal gravimetry. Rietveld structure refinement has permitted to localize inside the microporosity zirconium and oxygen atoms of extraframework clusters (EFCs), whose conformation depended on the nature of the zirconium precursor. Dissolution-condensation processes of $ZrCl_4$ and $ZrOCl_2$ during the synthesis gave rise to Zr_6 EFCs in one of every six cuboctahedral pores. Less numerous zirconia-like Zr_{12} oxo-clusters were formed from Zr isopropylate, whereas characteristic Zr_8 nitro-clusters were formed from Zr oxonitrate. The distances between oxygen atoms of EFCs and framework were compatible with the presence of additional TDC linkers connected to the EFCs. The results have been interpreted in terms of competition between Zr species during the condensation of the MOF network.

1. Introduction

Metal-organic frameworks (MOFs) constructed by metal nodes (ions/clusters) and organic linkers via coordination bonds possess many advanced properties such as large specific surface area, high pore volume, wide range of uniform pore size. Furthermore, there is a huge diversity in types of metal nodes/organic ligands, and easily tailorable functionalization; making MOFs as potential materials for various applications including gas adsorption/separation, [1,2] catalysis, [3–5] detection/sensing, [6,7] drug delivery, [8–11] and luminescence. [12–14] Unfortunately, the stability of a large number of MOFs in water or at high temperatures (e.g. > 350 ^{o}C) is inadequate for several applications in catalysis and adsorption/separation. [15–19] The stability towards hydrolysis of the bond between inorganic clusters and organic linkers is a critical parameter. [20] Improved water-resistance has been observed for MOFs with continuous inorganic chains, imidazolate linkers or high-coordination number inorganic clusters. [21–24] Prominent members of this last group are Zr(IV)-based MOFs, discovered in 2008, in which

strong coordination bonds between Zr^{4+} and the oxygen atoms of organic carboxylate linkers significantly improves chemical and thermal stability in comparison with other MOFs. [25] Their pore structure can be tuned by the use of appropriate organic modulators. [26–28] This has widened the field of application of Zr-MOFs in adsorption/separation processes. [27,29,30] The possibility of modification of both metal clusters and organic ligands has opened several applications as catalysts. [31,32]

DUT-67, where DUT stands for the Dresden University of Technology, is a more recent addition to the family of Zr-MOFs, with composition Zr_6O_8 $(TDC)_4$ $(OAc)_2$ $2H^+$, where TDC is 2,5-thiophenedicarboxylate and OAc is a carboxylic acid. The structure of DUT-67 is formed by 8-connected Zr_6-clusters $[Zr_6(\mu_3\text{-}O)_6(\mu_3\text{-}OH)_2]^{10+}$ bridged by TDC linkers in **reo** topology (Figure 1). [33] The DUT-67 structure, in the $Fm\bar{3}m$ (225) space group, presents two large microporous cavities: an octahedral cavity with width of 1.16 nm and a cubo-octahedral cavity with size of 1.42 nm. The smaller cavities are connected to the larger ones by 0.65 nm windows and the large cavities communicate through 0.85 nm windows. Catalytic metal active sites can be introduced in DUT-67 via impregnation. [34] Indeed, the thiophene group of the linker can coordinate metal cations (Figure SI1) making DUT-67 a potential adsorbent for the removal of heavy metal cations in wastewater treatment. [35,36] These post-synthesis treatments are made easier by the water-resistance of DUT-67, a property that allows the use of the material in heat pumps based on water vapour cycling. [37]

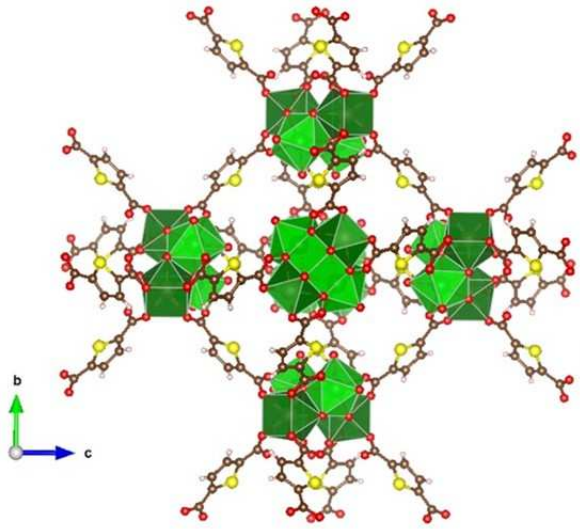

Figure 1. Structure of DUT-67. Zirconium atoms of the node clusters are represented by green coordination polyhedra. Colours of linker atoms: oxygen (red), sulfur (yellow), carbon (brown), hydrogen (grey).

The Zr_6 node clusters, beside the 8-coordination to the linkers, present two extraframework coordination oxygens, mainly pertaining to modulator or solvent molecules, which can be substituted by other monocarboxylate anions. This is a key point for the exchange of functional species into the DUT-67 structure, as it allows to form functionalized materials with remarkable performances in heterogeneous asymmetric catalysis and separation processes. [38,39] In as-synthesized DUT-67, a fraction of the coordination sites of the Zr_6 nodes are not connected to framework linkers but supplementary TDC linkers, connecting the Zr_6 node to additional disordered zirconium clusters. DUT-67 prepared in the original synthesis, in which acetic acid was used as a modulator and $ZrCl_4$ as a zirconium precursor, presented a supplementary Zr_6 clusters in nearly one of every four cubooctahedral cavities. [33] Soaking in water allowed the hydrolysis of the extraframework clusters (EFCs), without affecting the stability of the framework but leaving in the porosity some disordered extraframework matter. [33] Drache *et al*

showed that DUT-67 can be formed also in the presence of different modulators, such as formic or propionic acids, but no details were given on the formation of EFCs in these conditions. [26,40,41] A significant variability of the formation of EFCs with synthesis conditions was observed when DUT-67 was synthesized in aqueous solvent. [42] In this case, no EFCs were observed in the cubooctahedral cavity but a significant residual electron density was observed in the octahedral cavity. Residual electron density in cavities was also observed for DUT-67 synthesized with 1-H-pyrazole-3,5-dicarboxylic acid as a linker and $ZrO(NO_3)_2$ precursor, as well as in syntheses of UiO-66, Zr-fumarate, and Zr-mesaconate, suggesting extra-framework matter as a frequent occurrence in Zr-based MOFs. [42,43]

The importance of DUT-67 materials in the field of catalytic applications has been widened by total or partial replacement of Zr by Ce or Hf. [33,43–45] The improvement of the environmental impact and the scalability of Zr-MOF syntheses has received wide attention, notably implying microwave heating in an aqueous solvent and continuous synthesis in microfluidic systems. [46,47] In this context of growing interest, virtually no attention has been given to the nature and formation of EFCs, despite their potential relevance for the properties of the materials, from the porosity to the affinity for adsorbed species in separation and catalysis processes. In a first attempt to assess the variability of EFCs in Zr-based MOFs as a function of the preparation conditions, the present study is focused on the assessment of the nature of EFCs formed in DUT-67 synthesized from different metal precursors in the presence of a formic acid modulator.

2. Materials and Methods

Chemicals. All chemicals used in this study were purchased from Sigma Aldrich. Four zirconium precursors were studied, including zirconium (IV) chloride $ZrCl_4$ (99.9%), zirconium (IV) oxide chloride octahydrate $ZrOCl_2.8H_2O$ (98%), zirconium (IV) oxynitrate hydrate

$ZrO(NO_3)_2.xH_2O$ (99%), and zirconium (IV) propoxide solution 70 wt.% in 1-propanol. 2,5 thiophene dicarboxylic acid (H_2TDC) was used as the ligand. Formic acid ((FA); 98%) was used as the modulator, while dimethylformamide (DMF; 99.8%) and N-methyl-2-pyrrolidone (NMP; 99%) were used as solvents. The hydration *x* value in $ZrO(NO_3)_2.xH_2O$ was approximately 6, as determined from the mass loss in thermal gravimetric analysis (TG).

***Synthesis of DUT-67 analogues from different zirconium precursors*.** The synthesis protocol was inspired by Drache *et al*. with some modifications. [40] The solvent used for the syntheses was an equal volume mixture of DMF and NMP. In a typical experiment, 1.38 g of $ZrCl_4$ (6 mmol) was dissolved in 75 mL of the solvent solution before being mixed with 27 mL of formic acid (FA) to form solution A (n_{FA}/n_{Zr} ~ 120). Meanwhile, solution B was prepared by dissolving 0.663 g H_2TDC into 75 mL of the solvent mixture. Subsequently, solution B was mixed with solution A and further sonicated for 5 min. The resulting mixture was poured into 50 mL bottles (Schott Duran) that were then tightly closed and placed in an oven at 80 ºC for five days. A white solid was collected from the bottles, centrifugated and washed three times with DMF and then three times more with ethanol. Finally, the solid product was dried in an oven at 80 ºC for 12 h and then activated under vacuum at 120 ºC for 12 h. The obtained sample was denoted as C-FA (C and FA stand for $ZrCl_4$ precursor and formic acid modulator, respectively). The same synthesis procedure was used to produce other materials, in which $ZrCl_4$ was replaced with the molar equivalent of $ZrOCl_2.8H_2O$ (1.912 g), $ZrO(NO_3)_2.6H_2O$ (2.013 g), or $Zr(OCH_2CH_2CH_3)_4$ (2.778 g). The obtained products were denoted as OC-FA, N-FA, or OP-FA, respectively. Significant molar ratios of the syntheses are collected in Table 1, for easier comparison with literature data.

Table 1. Composition of the synthesis batches.

sample	source of Zr	modulator	modulator/Zr molar ratio	linker/Zr molar ratio
C-FA	$ZrCl_4$	formic acid	121	0.65
OC-FA	$ZrOCl_2{\cdot}8H_2O$	formic acid	121	0.65
N-FA	$ZrO(NO_3)_2{\cdot}6H_2O$	formic acid	115	0.62
OP-FA	$Zr(OCH_2CH_2CH_3)_4$	formic acid	116	0.63

All syntheses: 80°C, 4 days in isovolume dimethylformamide and N-methyl-2-pyrrolidone with Zr 39 mmol L^{-1}

***Characterization techniques*.** Powder X-ray diffraction (PXRD) patterns were obtained using a D8 Advance Diffractometer (Bruker AXS, Germany, CuK_α radiation and a Ni filter) in the Bragg–Brentano θ-θ geometry.

The measurements were performed in 2θ range of 2-40 °2Θ (angular step size of 0.0105 °2Θ and scanning rate of 0.63 per min) in order to well highlighted the peaks at low 2θ angles less affected by overlap that observed at higher diffraction angles. For all systems, the structure determination from powder X-ray diffraction data was carried out according to the procedure suggested by Martì-Rujas. [48] Indexing was performed by using N-TREOR09, as implemented in the EXPO program suit, in order to extract the integrated intensities of the powder diffraction patterns and to solve crystal structures via direct methods. [49] The experimental X-ray diffraction patterns collected were compatible with the $F\,m\bar{3}\,m$ space group (225) and the unit-cell parameters of DUT-67 reported by Bon et al. [33] All structure refinements were performed using the software GSAS implemented into the EXPGUI interface starting from the structural model reported by Bon et al. [33] Peak profiles were modeled by a pseudo-Voigt function, with

the peak cut-off set to 0.01% of the peak maximum, using three Gaussian terms (i.e., GU, GV, and GW, respectively), and the two Lorentzian broadening coefficients (i.e., LX, and LY, respectively). The background was empirically fitted with a Chebyshev polynomial function with 18 shifted coefficients (C-FA: $R_{wp}=0.078$, $R_p=0.063$, $R_F^2=0.065$; OC-FA: $R_{wp}=0.063$, $R_p=0.048$, $R_F^2=0.045$; OP-FA: $R_{wp}=0.067$, $R_p=0.048$, $R_F^2=0.58$; N-FA: $R_{wp}=0.058$, $R_p=0.045$, $R_F^2=0.046$).

Besides, scale factor and 2θ zero shift were also refined for both histograms. ADPs for atoms hosted at the same coordination site were imposed to be equal and constrained to change identically. All Rietveld refinements were performed by fixing the occupancy of the framework linker molecules to 1, hence assuming an ideal framework composition. A close inspection of the residual electron density was carried out by means of the Fourier and difference Fourier maps to highlight the occurrence of extraframework species in cuboctahedral cavities. The most electron density was assigned to supplementary Zr ions and their occupancy was refined in all structure refinement up to convergence. At this point, the match of the calculated diffraction pattern to the observed one revealed the occurrence of several peaks describing the occurrence of extraframework Zr oxo, oxy or oxonitrate ligands whose geometry was then optimized by plane wave DFT with dispersion correction (DFT-D), using the geometry optimization tool implemented in EXPO2014. [50] This approach allowed us to provide reasonable coordinates then used as input for GSAS and refined again several times until the geometry of the clusters were reasonable and the structural model showed the best agreement with the experimental data. In order to secure stable refinements, atomic coordinates were fixed in the final cycles of Rietveld refinement, thus limiting the number of refined atomic displacement parameters. Extraframework atomic coordinates were refined imposing soft constraints on C–C (*i.e.*, 1.40 Å, σ = 0.04 Å), C–O (*i.e.*, 1.25 Å, σ = 0.04 Å) and S-C bond distances (*i.e.*, 1.69 Å, σ = 0.04 Å) and

left free in the last cycles. The occupancies of individual atoms were constrained to be fixed considering the Zr EF content and their site multiplicity. No peaks larger than ±0.46 $e^{-1}/\approx Å^3$ were present in the final difference Fourier maps (Residuals (e $Å^{-3}$) C-FA: *-0.435/+0.455;* OC-FA: *-0.498/+0.333*; OP-FA-0.402/+0.375; N-FA: *-0.345/+0.333*). Details are reported in 3.2. section. Positions and occupancies of the C-FA, OC-FA, OP-FA and N-FA observed sites in or activation under vacuum at 120 °C are reported in **Table 2**.

Unit cell parameters, selected bond distances and bond angles are reported in Table 3, Table 4, Table SI1 and Table SI2, respectively**.** Unit cell parameters and selected bond distances of the C-FA, OC-FA, OP-FA and N-FA observed sites after drying at 80 °C are reported in Table SI3 and Table SI4, respectively. Positions of framework individual atoms in C-FA, OC-FA, OP-FA and N-FA samples after drying at 80 °C are reported in Table SI5-SI8.

Table 2. Coordinates and occupancy of extraframework sites.

	Atom	x/a	y/b	z/c	Multiplicity	Fraction
C-FA	Zr3	0	0.4220	0	24	1/3
	O7	0.0265	0.3999	0.0265	96	1/3
	O8	0.0350	0.4650	0.0350	32	1
OC-FA	Zr3	0	0.429	0	24	1/3
	O7	0.0332	0.3975	0.0332	32	1
	O8	0	0.0450	0.4500	96	1/3
OP-FA	Zr3	0.0562	0.4438	0	48	0.229
	O7	0.0250	0.4750	0.0250	32	0.703
	O8	0.0299	0.4040	0.0299	96	0.469
	O9	0.0980	0.4750	0.0980	96	0.234
N-FA	Zr3	0.4662	0.0338	0.0338	32	0.345

N1	1/2	0.0796	0.0796	48	0.345
O7	1/2	0.1010	0.1010	48	0.422
O8	0.0833	0.4509	0	96	0.211
O9	1/2	0	0	4	1
O10	0.4333	0.0667	0.0667	32	1

Morphology of the DUT-67 samples was analyzed by scanning electron microscopy (SEM) using a Hitachi S2600N microscope (Hitachi, Japan). Average size and size distribution were statistically determined by measuring sizes of more than 100 particles using ImageJ software. The textural properties of the materials were determined by nitrogen sorption isotherm measurements at 77.4 K using a Micromeritics Tristar instrument. Prior to each analysis, 50 mg of sample was outgassed at 120 ^{o}C for 16 h. The equivalent specific surface area was calculated using the Brunauer-Emmett-Teller (BET) model while the pore volume was assessed using the αS method.

Thermal gravimetric (TG) measurements were analyzed using a TA Instruments SDT Q600 Thermal Gravimetric Analyzer. In each experiment, 15 mg of the sample was placed in alumina pan and heated from 40 to 900 ^{o}C with a ramping rate 10 ^{o}C min^{-1} under 60 mL min^{-1} of air flow.

3. Results and discussion

DUT-67 network as a function of zirconium precursor. The powder X-ray diffraction patterns of the samples prepared using different zirconium precursors are shown in **Figure 2**. The X-ray powder diffraction patterns reveal crystalline DUT-67 materials regardless of the zirconium precursors. The unit cell parameters of the samples after activation under vacuum at 120 °C are reported in **Table SI3 and Table 3,** respectively. The unit cell dimensions are in the range 38.64-38.90 Å, slightly but significantly shorter than the 39.12 Å value observed by Bon *et*

al. for DUT-67 synthesized from $ZrCl_4$ in the presence of acetic acid. [33] A similar unit cell parameter 38.65 Å was already measured on DUT-67 synthesized from $ZrCl_4$ in the presence of formic acid and exchanged by HCl. [41] It is interesting to compare the distances between framework atoms of our samples (**Table SI1**) with the literature data for an acetic-acid synthesized sample. The values are very similar, but slight differences can account for variations in unit cell parameters. Rietveld structure refinements highlight slight differences in the unit cell parameters as well as in the average Zr-O distances (Zr1-O3 and Zr2-O1 are respectively, 0.14 and 0.06 Å) and bond angles respect those reported in the acetic-acid synthesized sample. A visual guide to the bonds is provided in **Figure SI1**. These variations could be related to a higher polarity of the outgassed samples prepared in the presence of formic acid. A similar unit cell parameter 38.65 Å was already measured on DUT-67 synthesized from $ZrCl_4$ in the presence of formic acid and exchanged by HCl. [41]

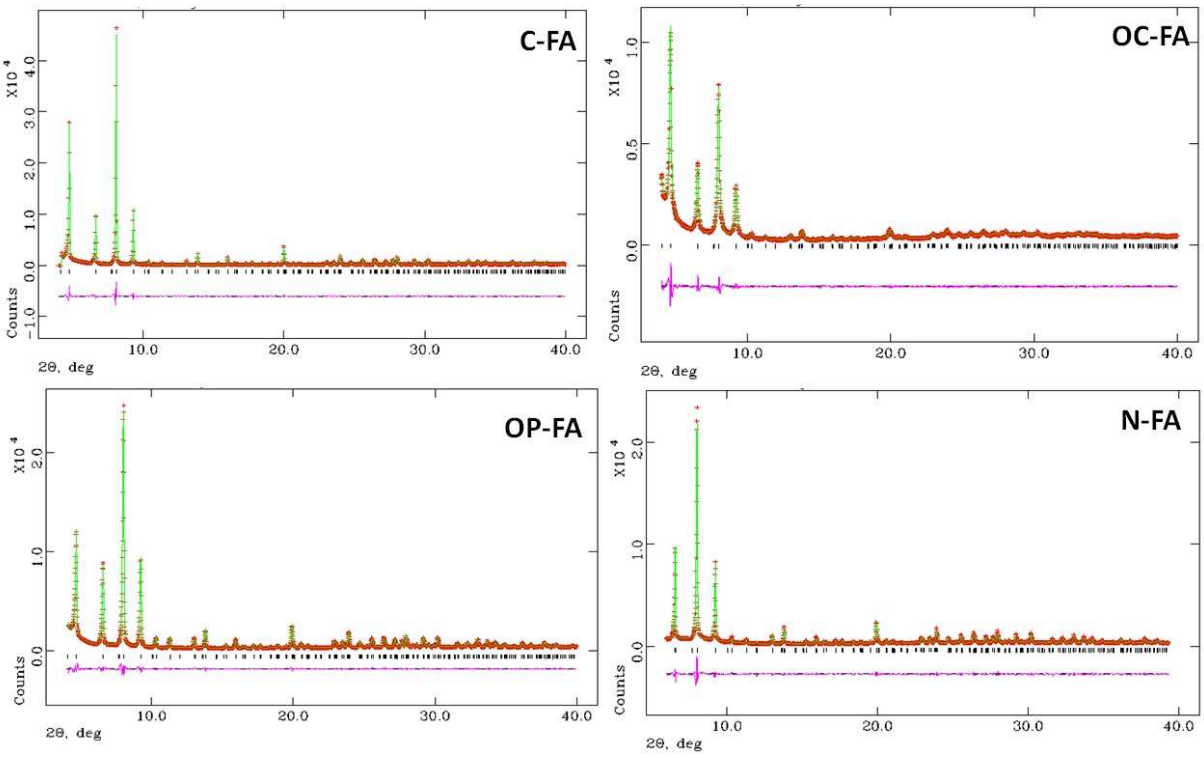

Figure 2. Rietveld refinement performed on X-ray powder diffraction data of the materials synthesized using different zirconium precursors: C-FA, $ZrCl_4$; OC-FA, $ZrOCl_2$; OP-FA, $Zr(OCH_2CH_2CH_3)_4$; N-FA, $ZrO(NO_3)_2$. The experimental data are indicated by cross signs, the calculated pattern is the continuous line and the lower curve is the weighted difference between the calculated and observed patterns.

***Extraframework clusters in cuboctahedral cavities*.** In C-FA sample, three crystallographically independent and partially occupied sites (labelled Zr3, O7 and O8, respectively) have been localized near the center of the cuboctahedral pore (**Figure 3** and **Table 2**).

The Zr3 site (*x/a = 0.0, y/b = 0.422, z/c = 0.0)* was eight-fold coordinated to O7 [x4] and O8 [x4], forming a Zr_6 EFC (**Figure 3 and Table 4**) with P*4mm* symmetry. Zr3 was connected to O7 and O8 in a distorted square antiprism configuration, as presented by isolated zirconium clusters [51] or by Zr1 and Zr2 in the framework node. The Zr_6 EFC symmetry was higher than the Zr_6 node cluster, likely been less constrained by ligands.

Table 3. Unit cell size of the prepared materials and CCDC deposition numbers.

		Deposition number	
Material	Cell size / Å	Activation at 80°C	Activation at 120°C
C-FA	38.895(1)	2085081	2085084
OC-FA	38.636(1)	2085088	2085087
OP-FA	38.889(1)	2085085	2085083
N-FA	38.838(1)	2085082	2085086

The refined occupancies indicated that the Zr EFC content corresponded to ~8 atoms per unit cell (a.u.c.), suggesting the occurrence of EFC in nearly one of six cuboctahedral cavities. This extraframework zirconium amount was in good agreement with what observed by Bon *et al.* on DUT-67 synthesized from $ZrCl_4$ in the presence of acetic acid as a modulator. [33]

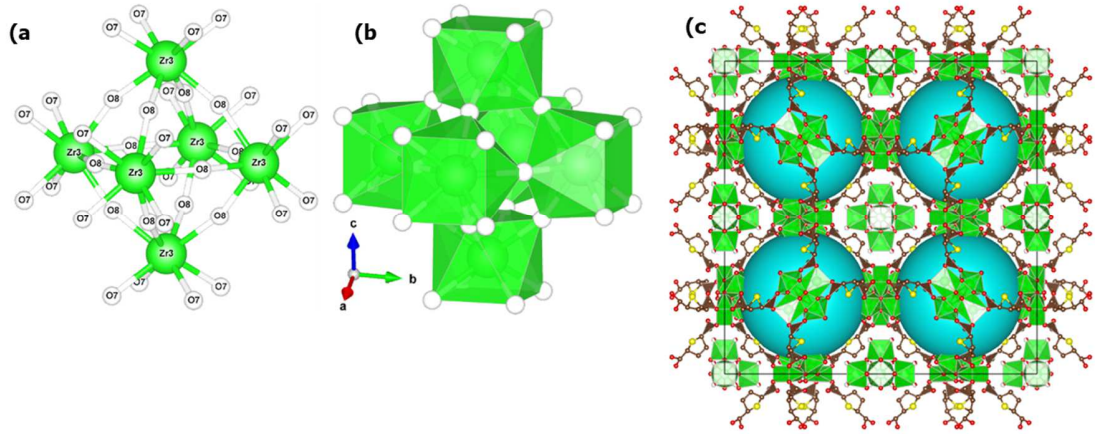

Figure 3. Extraframework cluster (EFC) in C-FA sample: (a) stick-and-ball and (b) coordination polyhedra representation; (c) location in the cuboctahedral pore (light blue spheres: octahedral pores).

Table 4. Significant distances (Å) between atoms of extraframework clusters

	C-FA	OC-FA	OP-FA	N-FA
Zr3-O7	2.24[x4]	2.18[x4]	1.974[x2]	
Zr3-O8	2.17[x4]	2.01[x4]	2.189[x4]	2.404[x6]
Zr3-O9			2.494[x2]	2.272
Zr3-O10				2.213

It has been suggested by Bon *et al.* that EFC in DUT-67 synthesized in acetic acid media are connected to the framework by additional TDC linkers. [33] In this case, it can be expected that,

also for C-FA, a significant fraction of external oxygens of the EFC pertain to carboxylate ligands connected to the framework (Table SI1). Indeed, the average distance between the external O7 oxygens of the EFC and the O3 and O5 oxygens of the core cluster was 7.36 Å, near the 7.27 Å distance normally observed between terminal oxygens of the framework TDC linker. It has not been possible to determine the position of the atoms of the linkers connecting the EFC to the core clusters, as expected due to their fractional disordered occupancies.

A very similar distribution of extraframework sites was observed on the OC-FA sample, synthesized using $ZrOCl_2 \cdot 8H_2O$ and formic acid modulator (**Table 3** and **Figure 4**). Zr3 additional ions (localized at *x/a = 0.0, y/b = 0.429, z/c = 0.0*) were coordinated to O7 and O8 atoms in the same configuration as in C-FA EFC. The Zr3-O mean distance was equal to 2.10 Å, slightly smaller than the 2.20 Å observed in C-FA (see **Table 4**). Also in this case, the overall Zr3 content detected in the cuboctahedral pore was ~8 Zr a.u.c. The average distance between the external O7 oxygens of the EFC and the O3 and O5 oxygens of the core cluster was 7.24 Å, also compatible with a connection of the EFC to the core cluster through a TDC linker.

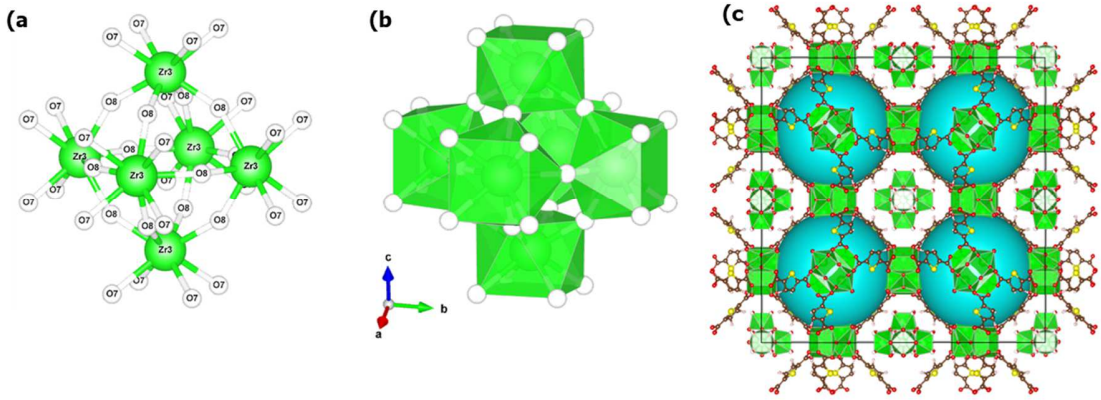

Figure 4. Extraframework cluster (EFC) in OC-FA sample: (a) stick-and-ball and (b) coordination polyhedra representation; (c) location in the cuboctahedral pore (light blue spheres: octahedral pores).

A different scenario has been observed in OP-FA sample. In fact, the difference Fourier map highlighted the occurrence of four extraframework sites (Zr3, O7, O8, O9) located in the cuboctahedral pore (**Table 3** and **Figure 5**). They formed a cuboctahedral Zr_{12} cluster, more condensated than either the usual Zr_6 cluster or the dimeric Zr_{12} cluster formed by two Zr_6 clusters connected by organic ligands. [52] [53] Here, the extra-framework Zr (at *x/a = 0.056, y/b = 0.443 z/c = 0.0*) was eightfold coordinated to four O8, two O7 and two O9 oxygens. The cuboctahedral clusters observed in OP-FA suggested analogies with a polyoxometallate configuration, as observed in Zr_{13} oxo-methoxo clusters. [54] Indeed, the Zr_{12} EFC presented a slightly distorted ZrO_2 structure, as the Zr3 site (local symmetry 2/m) can be derived from the Zr site of tetragonal zirconia by a protrusion of the external O9 oxygens.

Looking at possible connections between EFC and framework, the distances O8-O5 (6.81 Å) and O9-O3 (6.89 Å) seemed compatible with the presence of a bridging TDC linker. The sum of O9-O9 (10.95 Å), O9-O4 (4.48 Å) and O9-O5 distances (4.68 Å) corresponded to the 20.31 Å diagonal of the cubooctahedral pore, as expected by a centre of EFC near the centre of the cuboctahedral pore. The larger size of the cluster brought Zr atoms closer to the framework. The refined occupancies give rise to ~11 Zr EFC atoms per unit cell (a.u.c.), corresponding to an EFC in ~1/8 of the cuboctahedral pores.

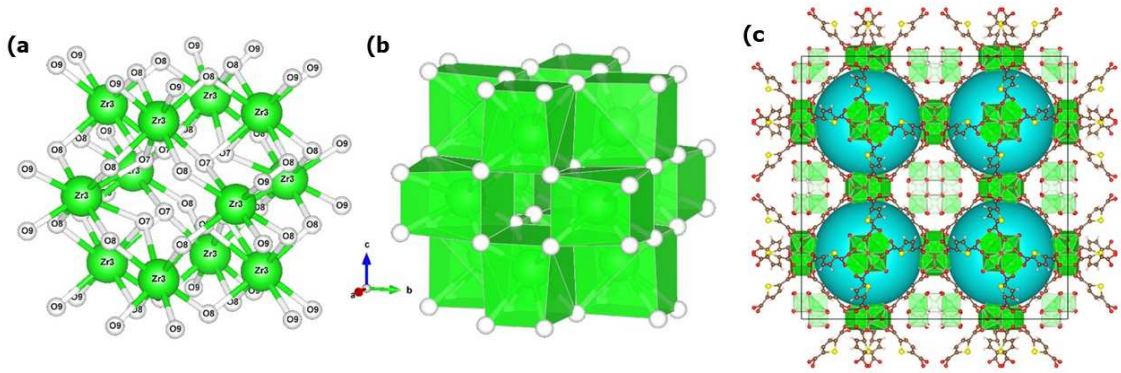

Figure 5. Extraframework cluster (EFC) in OP-FA sample: (a) stick-and-ball and (b) coordination polyhedra representation; (c) location in the cuboctahedral pore (light blue spheres: octahedral pores).

In N-FA, difference Fourier maps highlighted the occurrence of five significant electron density residuals, all located in the large cuboctahedral pores, with no similarity with the Zr clusters observed in other samples. The most intense residual peak (at about *x/a = 0.466, y/b = 0.034, z/c = 0.034)* has been assigned to Zr ions (Zr3 site). Other additional crystallographically independent sites have been assigned to NO_3^- groups (N, O7 and O8) and two Zr-linked oxygens (O9 and O10), coordinated to Zr3 (Zr3-O8=2.41[x6]Å, Zr3-O9=2.27Å, Zr3-O10=2.21Å) (Figure 6) in a flattened hexagonal bipyramid geometry, suggesting a local 6mmm symmetry. A cubic Zr8 cluster was formed by eight hexagonal bipyramids centered on the ternary axes of the cube, linked by bridging O7 oxygens and a central octa-coordinated O9. The coordination to a Zr(IV) cation of three bidentate nitrate groups around a ternary axis was reported as common in monomeric hydroxonitrate complexes. [55] The formation of the Zr_8 cluster probably involved interactions analogous to the formation of chains or tetramers of Zr hydroxynitrate dodecahedra as precursors of zirconia solvothermal synthesis. [56–58]

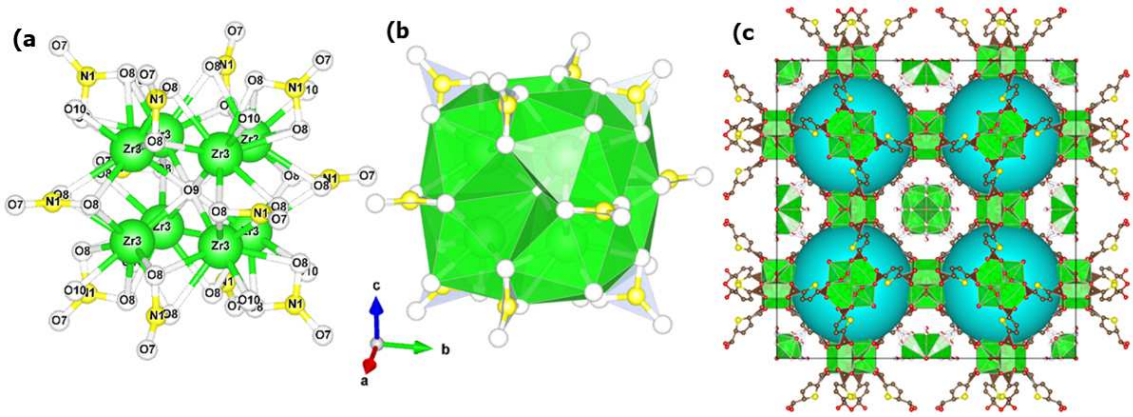

Figure 6. Extraframework cluster (EFC) in N-FA sample: (a) stick-and-ball and (b) coordination polyhedra representation; (c) location in the cuboctahedral pore (light blue spheres: octahedral pores).

The NO_3^- refined occupancies account for ~2.4 % in weight, whereas the Zr content in the cuboctahedral pores gives rise to ~11 atoms per unit cell (a.u.c.), corresponding to about one EFC of every six cuboctahedral pores. The refined O4-O10 distance (6.79 Å) suggested that also the Zr_8 EFC can be involved in interactions with the framework cluster through bridging the TDC linker.

Textural properties of the materials. Variations of the zirconium precursor affected the structural and macroscopic properties of the materials in different ways. Structural related properties, as surface area and micropore volume, are scantily affected by the nature of the precursor. The textural properties of these materials have been investigated by nitrogen sorption at 77.4 K. The obtained sorption isotherms are shown in **Figure 7** and textural data are reported in **Table 5**. Typical Type I sorption isotherms have been obtained, which is the indication of a microporous material. The sorption isotherm is fully reversible, as usually found for pure microporous materials.

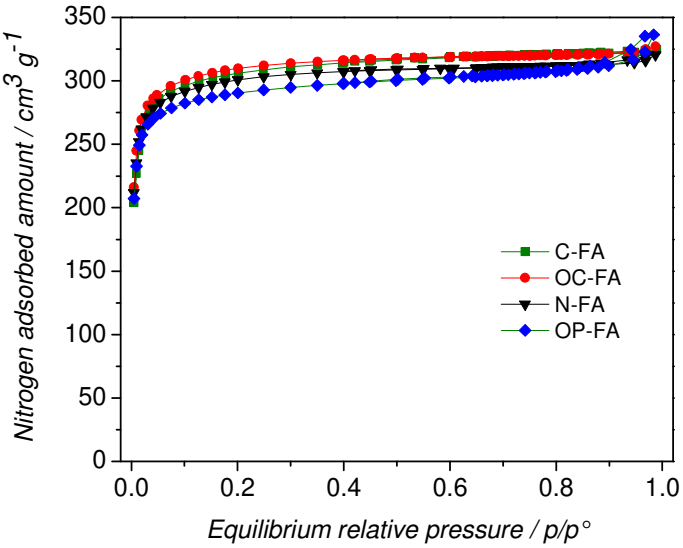

Figure 7. Nitrogen sorption isotherms of the DUT-67 materials prepared using different zirconium precursors.

Table 5. Textural properties of the materials

Parameter	C-FA	OC-FA	OP-FA	N-FA
BET surface area / $m^2\ g^{-1}$	1234	1248	1170	1198
External surface area / $m^2\ g^{-1}$	9	9	38	11
Micropore volume / $cm^3\ g^{-1}$	0.46	0.47	0.43	0.46
Mesopore volume / $cm^3\ g^{-1}$	0.04	0.03	0.08	0.03
Crystallite size by SEM / nm	887	503	168	596
Crystallite size by XRD / nm	196	116	80	186

Specific surface areas and pore volumes as high as 1143 $m^2\ g^{-1}$ and 0.47 $cm^3\ g^{-1}$ have already been measured on DUT-67 prepared in the presence of formic acid modulator, corresponding to the higher surface areas reported for this class of materials. [40] Our values of surface area, in the range 1170-1234 m^2g^{-1}, are marginally higher than the literature data. The nature of the

source of zirconium brought only minor modifications of the textural properties. C-FA and OC-FA have identical shapes of sorption isotherms. N-FA and OP-FA present slightly lower saturation plateaus, as demonstrated by their corresponding micropore volumes. The flatness of the saturation is related to the extent of external surface. If the saturation plateaus are truly horizontal, the external surface is negligible, compared to the specific surface area. Indeed, once micropores are filled with nitrogen, other sorption processes are unimportant. This is precisely the case of C-FA, OC-FA and N-FA. They, therefore, possess large micropore surfaces compared to their external surface, which means that these materials are made of large particles. OP-FA presents a steeper saturation plateau, corresponding to a significant external surface area, due to smaller particle size. A hysteresis loop at high relative pressure in the isotherm of OP-FA indicates that the agglomeration of the particles has originated a significant interparticular mesopore volume (see **Table 5**).

The low-pressure part of the adsorption isotherms also presents some interest. Semilogarithmic plots of the sorption isotherms are reported in **Figure SI2** and indicate that nearly half the micropore volume is filled at p/p° 1E-3. This value can be compared with the relative pressure of adsorption of N_2 at 77 K in faujasite, a zeolite whose supercages present a diameter of 11.7 Å, comparable with the 11.7 and 14.2 Å cages of DUT-67. N_2 adsorption is centered at p/p° 1E-6 on aluminium-rich Na-X and between 1E-4 and 1E-3 on pure silica faujasite. [59,60]

These values suggest an analogy between the surface polarity of DUT-67 and highly hydrophobic pure silica faujasite, an effect which could contribute to the cited water-resistance of Zr-MOFs. A conformation of the low polarity of the DUT-67 micropore surface comes from the values of N_2 adsorption energy calculated by the Dubinin-Radushkevitch method. [61]

The values of adsorption energy reported in Table SI9 are near 5 KJ mol^{-1}, marginally smaller than the 7 KJ mol^{-1} values measured on dealuminated zeolites [62]

The SEM images reported in **Figure 8** highlight the smaller size and higher agglomeration of the OP-FA particles. The micrographs of all samples show a well-defined truncated octahedron morphology. The relative extent of the (100) and (111) faces varies from one sample to another. OC-FA features a nearly perfect cuboctahedron morphology, due to lesser development of the (111) faces, while the other samples present more extended hexagonal (111) faces. The larger development of the higher index (111) faces corresponds to slower growth of the cubic (100) faces.

The SEM images reported in **Figure 8** visually highlight the smaller size and higher agglomeration of the OP-FA particles, in agreement with the data of **Table 2**. Tentatively explanations can be proposed for this effect. Indeed, the propoxide anions are strongly basic and can rapidly deprotonate the fumaric acid as well as the thiophenedicarboxylic acid, thus leading to very fast nucleation and only a short growth process. Furthermore, these very small particles could be stabilized by the presence of propanol in the reaction mixture, originating from both the initial solution of zirconium propoxide (1-propanol as solvent) and by the formation *in situ* upon hydrolysis of the zirconium precursor. Such propanol species could prevent the growth of DUT-67 particles by their stabilization effect.

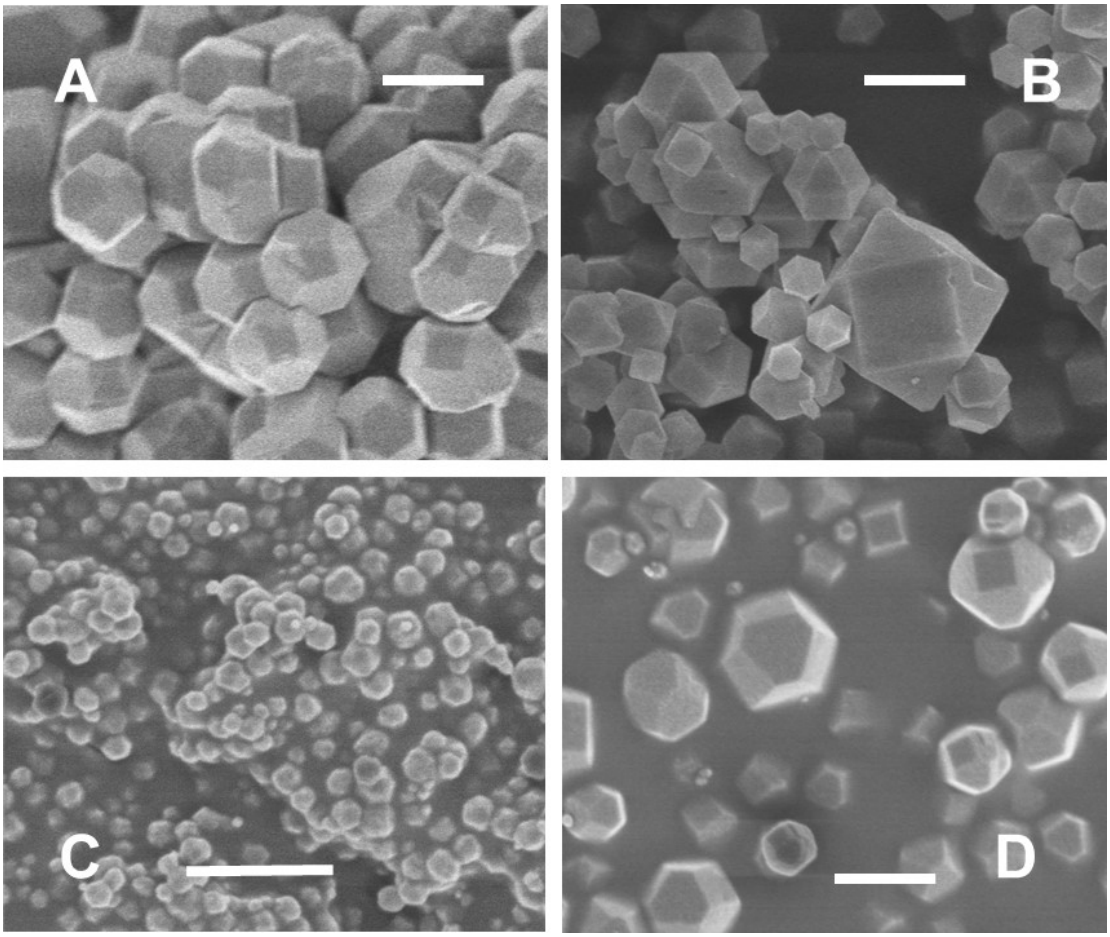

Figure 8. SEM micrographs of DUT-67 samples prepared from different zirconium precursors: C-FA (A), OC-FA (B), OP-FA (C), N-FA (D). The scale bar is 1 μm for each picture.

The data in **Table 2** indicate that, in all cases, the estimated particle size by image processing is significantly larger than the crystallite size by XRD, despite the well-defined single-crystal-like morphology of the particles. The most likely explanation for this effect is the fragmentation of the periodic domain, probably due to shrinkage mismatch between inner and outer parts of the crystals.

***Thermogravimetric results*.** The results of thermal gravimetry on the materials are shown in **Figure 9**. All samples follow a similar weight loss pattern (**Figure 9A**) in good agreement with literature reports on DUT-67. [25] Two weight-loss steps at 90 and 250 °C account for the loss of

20-25 % of the initial mass. A continuous loss of mass follows until a sudden loss at 430 °C brings the samples to 42-46 % of the initial mass. Further mass loss is observed between 600 and 800 °C. The attribution of the mass losses to specific phenomena is made easier by normalizing the data on the final mass instead than on the initial mass. In **Figure 9B**, the mass losses are expressed as $(m-m_f)/m_f$, *i.e.* as fractions of the final mass, where m is the mass at a given temperature and m_f is the mass at the end of the TG experiment. Assuming that the final mass corresponds to the amount of ZrO_2 formed in the oxidative degradation of DUT-67, some information on the mass loss phenomena can be deduced by the stoichiometry of the decomposition. The presence of EFCs is not expected to bring large variations in the TG pattern, as they represent no more than 8 % of the total zirconium and they are linked to a significant amount of non-framework linkers. The total oxidation of an ideal DUT-67, devoid of extraframework species, would correspond to the reaction $Zr_6O_8(C_6H_2O_4S)_4(CH_2O_2)_2 + 26\ O_2$ (gas) $\rightarrow 6\ ZrO_2 + 26\ CO_2$ (gas) $+ 6\ H_2O$ (gas) $+ 4\ SO_2$ (gas), which implies a mass loss $\Delta m/m_f = 0.96$. This value of the mass loss is reached between 310 and 345 °C according to the material. This suggests that mass losses below this temperature have to be attributed to volatile extraframework components. Tentative attributions can identify the mass loss below 120 °C with adsorption of atmospheric moisture and the next mass loss step with retained DMF and DMP solvents. It can be observed that the lower amount of retained solvent is observed on OP-FA, the sample with smaller crystals, suggesting easier outgassing of the material for shorter diffusion paths. The decomposition phenomena between 600 and 800 °C are in the temperature range expected for the thermal decomposition of zirconium or zirconyl sulphate. [63] The mass loss of 0.14-0.18 $\Delta m/m_f$ in this temperature range corresponds to a fraction of the mass loss expected for the reaction $ZrO(SO_4) + ½O_2 \rightarrow ZrO_2 + SO_2$, suggesting that a significant amount of SO_2 has

been emitted in the main thermal degradation phenomenon at 430 °C, in good agreement with the results of Drache *et al*. [41]

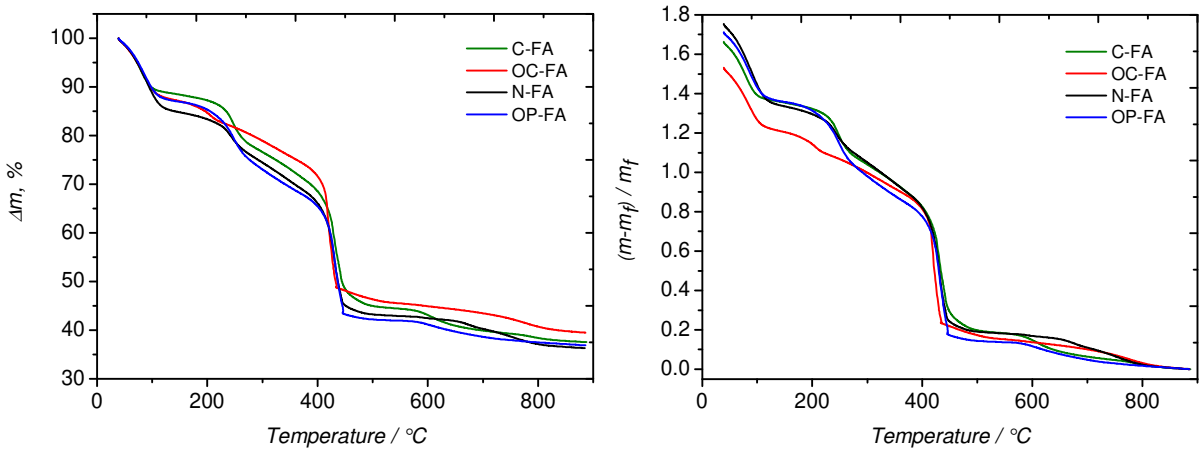

Figure 9. TG curves of DUT-67 samples prepared from different zirconium precursors.

***4. Relevance of the results*.** The speciation of node clusters plays an important role in the formation of MOFs. The number and symmetry of coordination sites in the nodes determine the topology of the MOF structure. In many cases, the chemistry of the synthesis medium univocally determines the properties of dissolved species able to coordinate with linkers to form a well-defined structure. In the development of MOF synthesis, the search for materials with improved performances has led to a move towards more complex node species. Zr-MOFs represent a clear example of how modifications of the synthesis environment lead to changes in node coordination and corresponding changes of network topology. The characterization and the definition itself of MOF materials are based on the assessment of the periodic properties of their network. In several instances, materials inside the porosity of a MOF network have been more difficult to characterize. A seminal instance has been the growth of MOFs' interpenetrating networks, indicating that the condensation of clusters and linkers can start from multiple nucleation sites, also inside the porosity of existing networks. [64,65]

In the case of Zr-MOF, the presence of an additional Zr cluster in fractional periodical position inside the porosity has been early recognized. [33] They correspond to supplementary coordination of linkers to some network clusters, leading to a local alternative configuration unable to develop in a periodic structure. In the synthesis of DUT-67 from $ZrCl_4$ with acetic acid modulator, the additional clusters have been identified as the same cluster, which forms the node of the periodic structure. Zr_6 clusters with Zr in square antiprism configuration are at the basis, in monomeric or dimeric form, of several MOF structures. It has been shown that moving from organic to aqueous solvent, the formation of extraframework additional clusters in the cuboctahedral cavity was prevented. [42,43]

The results of this paper show other examples of how the chemical environment can orient the formation of different zirconium clusters, highlighting the role of modulators and zirconium precursors. Alternative interactions with linkers, modulators and precursor anions lead to the formation of different zirconium species in the system. Zr_6 clusters with Zr in square antiprism configuration, forming both the periodical framework and EFCs, were the only ones observed when zirconium chloride or oxychloride were used as zirconium precursors (samples C-FA and OC-FA). In the synthesis from zirconium propionate or oxynitrate, EFCs with different configurations were detected. Also in these materials (OP-FA and N-FA) the usual Zr6 clusters were largely majority, forming the periodical framework of DUT-67 and representing more than 92% zirconium in the material. Zr_{12} clusters condensed after the dissolution of Zr propionate or Zr_8 clusters formed by condensation of dissolution products of Zr oxynitrate are present as EFCs in these materials. It is likely that these clusters were minority in the synthesis solution also before the condensation of the framework. Nevertheless, it is also possible that clusters able to form a periodic network had enjoyed a competitive advantage, the formation of the framework

subtracting them to equilibria in solution. Additional clusters in the porosity are likely leftovers of germs of alternative structures less able to grow in periodical networks than the usual Zr_6 clusters with Zr in square antiprism configuration. The search for conditions in which alternative ligands, issued from cation sources or purposefully added, can modify the cluster population in the synthesis system, opens fascinating prospects for the synthesis of new MOFs.

5. Conclusions.

The presence of residual precursors inside the porosity of MOFs has only recently received some attention. Zr-based MOFs have been especially relevant on this account, on the basis of the stability of their clusters. To our knowledge, we have reported here for the first time the identification of both cations and oxygens in extraframework clusters (EFCs) of DUT-67. The knowledge of the distances between oxygens of EFC and network sites has allowed to substantiate the proposed bridging of EFC to the framework by additional linkers, adding an element of complexity to the mechanism of condensation and crystallization of the materials. Also for the first time, a variety of zirconium oxoclusters has been found inside MOF micropores as a function of the synthesis precursors. This confirms that the speciation of Zr clusters and their competition for the insertion into the MOF structure is a field of research with high potential for further purposeful growth.

Credit author statement :

P.T., A.M. and F. D. R, K. D. N. and H. V. L: Conceptualization, Supervision, Writing – review and editing.

P. H; H, N. P., L. G., G. T., S. D.: Investigation, Methodology, Writing – original draft.

T.C. : XRD production.

Corresponding Authors :

* Philippe.trens@enscm.fr

* mrs@unife.it

Author Contributions

The manuscript was written through contributions of all authors. All authors have given approval to the final version of the manuscript.

ACKNOWLEDGMENT

PHH is grateful to the European FEDER Readynov Solarvi for financial support.

References

[1] J.R. Li, R.J. Kuppler, H.C. Zhou, Selective gas adsorption and separation in metal-organic frameworks, Chem. Soc. Rev. 38 (2009) 1477–1504.

[2] H. Belarbi, L. Boudjema, C. Shepherd, N. Ramsahye, G. Toquer, J.-S. Chang, P. Trens, Adsorption and separation of hydrocarbons by the metal organic framework MIL-101(Cr), Colloids Surfaces A Physicochem. Eng. Asp. 520 (2017) 46–52.

[3] D. Farrusseng, S. Aguado, C. Pinel, Metal-organic frameworks: Opportunities for catalysis, Angew. Chemie - Int. Ed. 48 (2009) 7502–7513.

[4] Y.K. Hwang, D.Y. Hong, J.S. Chang, S.H. Jhung, Y.K. Seo, J. Kim, A. Vimont, M. Daturi, C. Serre, G. Férey, Amine grafting on coordinatively unsaturated metal centers of MOFs: Consequences for catalysis and metal encapsulation, Angew. Chemie - Int. Ed. 47 (2008) 4144–4148.

[5] G. Férey, Hybrid porous solids: Past, present, future, Chem. Soc. Rev. 37 (2008) 191–214.

[6] L.E. Kreno, K. Leong, O.K. Farha, M. Allendorf, R.P. Van Duyne, J.T. Hupp, Metal-

Organic Framework Materials as Chemical Sensors, Chem. Rev. Rev. 112 (2012) 1105–1125.

[7] B. Liu, Metal-organic framework-based devices: Separation and sensors, J. Mater. Chem. 22 (2012) 10094–10101.

[8] P. Horcajada, C. Serre, M. Vallet-Regí, M. Sebban, F. Taulelle, G. Férey, Metal-organic frameworks as efficient materials for drug delivery, Angew. Chem. Int. Ed. Engl. 45 (2006) 5874–5878.

[9] P. Horcajada, T. Chalati, C. Serre, B. Gillet, C. Sebrie, T. Baati, J.F. Eubank, D. Heurtaux, P. Clayette, C. Kreuz, J.-S. Chang, Y.K. Hwang, V. Marsaus, P.-N. Borie, L. Cynober, S. Gil, G. Férey, P. Couvreur, R. Gref, Porous metal–organic-framework nanoscale carriers as a potential platform for drug delivery and imaging, Nat. Mater. 9 (2010) 172-178.

[10] J. Zhuang, C.-H. Kuo, L.-Y. Chou, D.-Y. Liu, E. Weerapana, C.-K. Tsung, Optimized Metal–Organic-Framework Nanospheres for Drug Delivery: Evaluation of Small-Molecule Encapsulation., ACS Nano. 8 (2014) 2812–2819.

[11] H. Zheng, Y. Zhang, L. Liu, W. Wan, P. Guo, A.M. Nyström, X. Zou, One-pot Synthesis of Metal-Organic Frameworks with Encapsulated Target Molecules and Their Applications for Controlled Drug Delivery, J. Am. Chem. Soc. 138 (2016) 962–968.

[12] L. Boudjema, G. Toquer, A.H. Basta, P. Trens, D.A. Lerner, Confinement-Induced Electronic Excitation Limitation of Anthracene: The Restriction of Intramolecular Vibrations, J. Phys. Chem. C. 122 (2018) 28416–28422.

[13] S. Furukawa, Y. Takashima, H. Uehara, V.M. Martínez, K. Sugimoto, S. Kitagawa, S. Shimomura, M. Nakahama, M. Kondo, Molecular decoding using luminescence from an entangled porous framework, Nat. Commun. 2 (2011) 168.

[14] M.D. Allendorf, C.A. Bauer, R.K. Bhakta, R.J.T. Houk, Luminescent metal-organic frameworks, Chem. Soc. Rev. 38 (2009) 1330–1352.

[15] P. Küsgens, M. Rose, I. Senkovska, H. Fröde, A. Henschel, S. Siegle, S. Kaskel, Characterization of Metal-Organic Frameworks by Water Adsorption, Micropor. Mesopor. Mat. 120 (2009) 325−330.

[16] S.K. Henninger, F.P. Schmidt, H.M. Henning, Water adsorption characteristics of novel materials for heat transformation applications, Appl. Therm. Eng. 30 (2010) 1692–1702. http://dx.doi.org/10.1016/j.applthermaleng.2010.03.028.

[17] T. Terencio, F. Di Renzo, D. Berthomieu, P. Trens, Adsorption of acetone vapor by Cu-BTC: An experimental and computational study, J. Phys. Chem. C. 117 (2013) 26156–26165. doi:10.1021/jp410152p.

[18] C. Wang, X. Liu, N. Keser Demir, J.P. Chen, K. Li, Applications of water stable metal–organic frameworks., Chem. Soc. Rev. 45 (2016) 5107–5134.

[19] L. Boudjema, E. Mamontova, J. Long, J. Larionova, Y. Guari, P. Trens, Prussian Blue Analogues for the Separation of Hydrocarbons in Humid Conditions, Inorg. Chem. 56 (2017) 7598–7601. doi:10.1021/acs.inorgchem.7b00563.

[20] J.J. Low, A.I. Benin, P. Jakubczak, J.F. Abrahamian, S.A. Faheem, R.R. Willis, Virtual high throughput screening confirmed experimentally: Porous coordination polymer hydration, J. Am. Chem. Soc. 131 (2009) 15834–15842.

[21] S. Aguado, J. Canivet, Y. Schuurman, D. Farrusseng, Tuning the activity by controlling the wettability of MOF eggshell catalysts: A quantitative structure–activity study., J. Catal. 284 (2011) 207–214.

[22] I.J. Kang, N.A. Khan, E. Haque, S.H. Jhung, Chemical and Thermal Stability of Isotypic Metal–Organic Frameworks: Effect of Metal Ions., Chem. - A Eur. J. 17 (2011) 6437–6442.

[23] J. Canivet, A. Fateeva, Y. Guo, B. Coasne, D. Farrusseng, Water adsorption in MOFs: Fundamentals and applications, Chem. Soc. Rev. 43 (2014) 5594–5617.

[24] J. Duan, W. Jin, S. Kitagawa, Water-resistant porous coordination polymers for gas separation, Coord. Chem. Rev. 332 (2017) 48–74.

[25] J.H. Cavka, S. Jakobsen, U. Olsbye, N. Guillou, C. Lamberti, S. Bordiga, K.P. Lillerud, A New Zirconium Inorganic Building Brick Forming Metal Organic Frameworks with Exceptional Stability, J. Am. Chem. Soc. 130 (2008) 13850–13851.

[26] A. Schaate, P. Roy, A. Godt, J. Lippke, F. Waltz, M. Wiebcke, P. Behrens, Modulated

Synthesis of Zr-Based Metal–Organic Frameworks: From Nano to Single Crystals., Chem. Eur. J. 17 (2011) 6643 – 6651.

[27] H. Furukawa, F. Gándara, Y.B. Zhang, J. Jiang, W.L. Queen, M.R. Hudson, O.M. Yaghi, Water adsorption in porous metal-organic frameworks and related materials, J. Am. Chem. Soc. 136 (2014) 4369–4381.

[28] F. Drache, V. Bon, I. Senkovska, J. Getzschmann, S. Kaskel, The modulator driven polymorphism of Zr(IV) based metal–organic frameworks, Philos. Trans. R. Soc. A Math. Phys. Eng. Sci. 375 (2017) 20160027.

[29] M.A. Moreira, J.C. Santos, A.F.P. Ferreira, J.M. Loureiro, F. Ragon, P. Horcajada, K.E. Shim, Y.K. Hwang, U.H. Lee, J.S. Chang, C. Serre, A.E. Rodrigues, Reverse shape selectivity in the liquid-phase adsorption of xylene isomers in zirconium terephthalate MOf UiO-66, Langmuir. 28 (2012) 5715–5723.

[30] N.A. Ramsahye, P. Trens, C. Shepherd, P. Gonzalez, T.K. Trung, F. Ragon, C. Serre, The effect of pore shape on hydrocarbon selectivity on UiO-66(Zr), HKUST-1 and MIL-125(Ti) metal organic frameworks: Insights from molecular simulations and chromatography, Microporous Mesoporous Mater. 189 (2014) 222–231.

[31] S.N. Kim, Y.R. Lee, S.H. Hong, M.S. Jang, W.S. Ahn, Pilot-scale synthesis of a zirconium-benzenedicarboxylate UiO-66 for CO2 adsorption and catalysis, Catal. Today. 245 (2015) 54–60.

[32] C. Caratelli, J. Hajek, F.G. Cirujano, M. Waroquier, F.X. Llabrés i Xamena, V. Van Speybroeck, Nature of active sites on UiO-66 and beneficial influence of water in the catalysis of Fischer esterification, J. Catal. 352 (2017) 401–414.

[33] V. Bon, I. Senkovska, I.A. Baburin, S. Kaskel, Zr- and Hf-Based Metal–Organic Frameworks: Tracking Down the Polymorphism, Cryst. Growth Des. 13 (2013) 1231–1237.

[34] G.L. Zhuang, J.Q. Bai, L. Tan, H.L. Huang, Y.F. Gao, X. Zhong, C.L. Zhong, J.G. Wang, Preparation and catalytic properties of Pd nanoparticles supported on micro-crystal DUT-67 MOFs, RSC Adv. 5 (2015) 32714–32719.

[35] S. Chen, F. Feng, S. Li, X.X. Li, L. Shu, Metal-organic framework DUT-67 (Zr) for

adsorptive removal of trace Hg2+ and CH3Hg+ in water, Chem. Speciat. Bioavailab. 30 (2018) 99–106.

[36] A.R. Geisse, C.M. Ngule, D.T. Genna, Removal of lead ions from water using thiophene-functionalized metal–organic frameworks, Chem. Commun. 56 (2020) 237–240.

[37] V. Bon, I. Senkovska, J.D. Evans, M. Wöllner, M. Hölzel, S. Kaskel, Insights into the water adsorption mechanism in the chemically stable zirconium-based MOF DUT-67 – a prospective material for adsorption-driven heat transformations, J. Mater. Chem. A. 7 (2019) 12681–12690.

[38] K.D. Nguyen, C. Kutzscher, S. Ehrling, I. Senkovska, V. Bon, T. de Oliveira, M. Gutmann, G. Buntkowsky, S. Kaskel, Insights into the role of zirconium in proline functionalized metal-organic frameworks attaining high enantio- and diastereoselectivity, J. Catal. 377 (2019) 41–50.

[39] K.D. Nguyen, C. Kutzscher, F. Drache, I. Senkovska, S. Kaskel, Chiral Functionalization of a Zirconium Metal–Organic Framework (DUT-67) as a Heterogeneous Catalyst in Asymmetric Michael Addition Reaction, Inorg. Chem. 57 (2018) 1483–1489.

[40] F. Drache, V. Bon, I. Senkovska, C. Marschelke, A. Synytska, S. Kaskel, Postsynthetic Inner-Surface Functionalization of the Highly Stable Zirconium-Based Metal-Organic Framework DUT-67, Inorg. Chem. 55 (2016) 7206–7213.

[41] F. Drache, F.G. Cirujano, K.D. Nguyen, V. Bon, I. Senkovska, F.X. Llabrés i Xamena, S. Kaskel, Anion Exchange and Catalytic Functionalization of the Zirconium-Based Metal−Organic Framework DUT-67, Cryst. Growth Des. 18 (2018) 5492−5500.

[42] H. Reinsch, S. Waitschat, S.M. Chavan, K.P. Lillerud, N. Stock, A Facile "Green" Route for Scalable Batch Production and Continuous Synthesis of Zirconium MOFs, Eur. J. Inorg. Chem. 2016 (2016) 4490–4498.

[43] J. Jacobsen, H. Reinsch, N. Stock, Systematic Investigations of the Transition between Framework Topologies in Ce/Zr-MOFs, Inorg. Chem. 57 (2018) 12820–12826.

[44] M. Lammert, C. Glißmann, R. H., N. Stock, Synthesis and Characterization of New Ce(IV)-MOFs Exhibiting Various Framework Topologies., Cryst. Growth Des. 17 (2017) 1125–1131.

[45] W. Li, Z. Cai, H. Li, Y. Shen, Y. Zhu, H. Li, X. Zhang, F. Wang, Hf-based metal organic frameworks as bifunctional catalysts for the one-pot conversion of furfural to γ-valerolactone, J. Mol. Catal. 472 (2019) 17–26.

[46] H. Reinsch, Green Synthesis of Metal-Organic Frameworks, Eur. J. Inorg. Chem. (2016) 4290–4299.

[47] Y. Wang, L. Li, L. Yan, L. Cao, P. Dai, X. Gu, X. Zhao, Continuous synthesis for zirconium metal-organic frameworks with high quality and productivity via microdroplet flow reaction., Chin. Chem. Lett. 29 (2018) 849–853.

[48] J. Martí-Rujas, Structural elucidation of microcrystalline MOFs from powder X-ray diffraction, Dalt. Trans. 49 (2020) 13897–13916.

[49] A. Altomare, C. Giacovazzo, A. Guagliardi, A.G. Moliterni, R. Rizzi, P.E. Werner, New techniques for indexing: N-TREOR in EXPO., J. Appl. Crystallogr. 33 (2000) 1180–1186.

[50] A. Altomare, N. Corriero, C. Cuocci, A. Falcicchio, A. Moliterni, R. Rizzi, EXPO software for solving crystal structures by powder diffraction data: methods and application., Cryst. Res. Tech. 50 (2015) 737–742.

[51] P. Piszczek, A. Radtke, A. Grodzicki, A. Wojtczak, J. Chojnacki, The new type of [Zr6(μ3-O)4(μ3-OH)4] cluster core: Crystal structure and spectral characterization of [Zr6O4(OH)4(OOCR)12] (R = But, C(CH3)2Et), Polyhedron. 26 (2007) 679–685.

[52] M. Puchberger, F.R. Kogler, M. Jupa, S. Gross, H. Fric, G. Kickelbick, U. Schubert, Can the Clusters Zr6O4(OH)4(OOCR)12 and [Zr6O4(OH)4(OOCR)12]2 be Converted into Each Other?, Eur. J. Inorg. Chem. (2006) 3283–3293.

[53] S.B. Peh, Y. Cheng, J. Zhang, Y. Wang, G.H. Chan, J. Wang, D. Zhao, Cluster nuclearity control and modulated hydrothermal synthesis of functionalized Zr12 metal–organic frameworks., Dalt. Trans. 48 (2019) 7069–7073.

[54] B. Morosin, Molecular configuration of a tridecazirconium oxide-methoxide complex., Acta Cryst. B. 33 (1977) 303–305.

[55] I. V. Morozov, A.A. Fedorova, D. V. Palamarchuk, S.I. Troyanov, Synthesis and crystal structures of zirconium (IV) nitrate complexes (NO2)[Zr(NO3)3(H2O)3]2 (NO3)3,

Cs[Zr(NO3)5], and (NH4)[Zr(NO3)5](HNO3)., Russ. Chem. Bull. 54 (2005) 93–98.

[56] P. Bénard-Rocherullé, J. Rius, D. Louër, Structural Analysis of Zirconium Hydroxide Nitrate Monohydrates by X-Ray Powder Diffraction., J. Solid State Chem. 128 (1997) 295–304.

[57] P.D. Southon, J.R. Bartlett, J.L. Woolfrey, B. Ben-Nissan, Formation and Characterization of an Aqueous Zirconium Hydroxide Colloid., Chem. Mater. 14 (2002) 4313–4319.

[58] C. Tyrsted, N. Lock, K.M.Ø. Jensen, M. Christensen, E.D. Bøjesen, H. Emerich, G. Vaughan, S.J.L. Billinge, B.B. Iversen, Evolution of atomic structure during nanoparticle Formation, IUCrJ. 1 (2014) 165–171.

[59] M. Thommes, K.A. Cychosz, Physical adsorption characterization of nanoporous materials: progress and challenges, Adsorption. 20 (2014) 233–250.

[60] A. Martin-Calvo, J.J. Gutierrez-Sevillano, J.B. Parra, C.O. Aniab, S. Calero, Transferable force fields for adsorption of small gases in zeolites, Phys. Chem. Chem. Phys. 17 (2015) 24048–24055.

[61] N.D. Hutson, R.T. Yang, Theoretical Basis for the Dubinin-Radushkevitch (D-R) Adsorption Isotherm Equation, Adsorption. 3 (1997) 189–195.

[62] M.J. Remy, G. Poncelet, A New Approach to the Determination of the External Surface and Micropore Volume of Zeolites from the Nitrogen adsorption Isotherm at 77 K, J. Phys. Chem. 99 (1995) 773–779.

[63] C.A. Strydom, J. Pretorius, The thermal decomposition of zirconium sulphate hydrate., Thermochim. Acta. 223 (1993) 223–232.

[64] B. Chen, M. Eddaoudi, S.T. Hyde, M. O'Keeffe, O.M. Yaghi, Interwoven Metal-Organic Framework on a Periodic Minimal Surface with Extra-Large Pores, Science (80-.). 291 (2001) 1021–1023.

[65] B. Li, Q.-Q. Yan, Z.-Q. Xu, Y.-B. Xu, G.-P. Yong, Tuning the interpenetration of metal–organic frameworks through changing ligand functionality: effect on gas adsorption properties., CrystEngComm. 22 (2020) 506–514.

Graphical abstract. The nature of extra framework clusters in DUT-67 can be driven by using the appropriate zirconium precursor. Here is reported for the first time the identification of both cations and oxygens in four types of extraframework clusters located in DUT-67 materials.